ISSN 1001-0742
CN 11-2629/X

JES

JOURNAL OF ENVIRONMENTAL SCIENCES

March 1, 2015 Volume 29
www.jesc.ac.cn

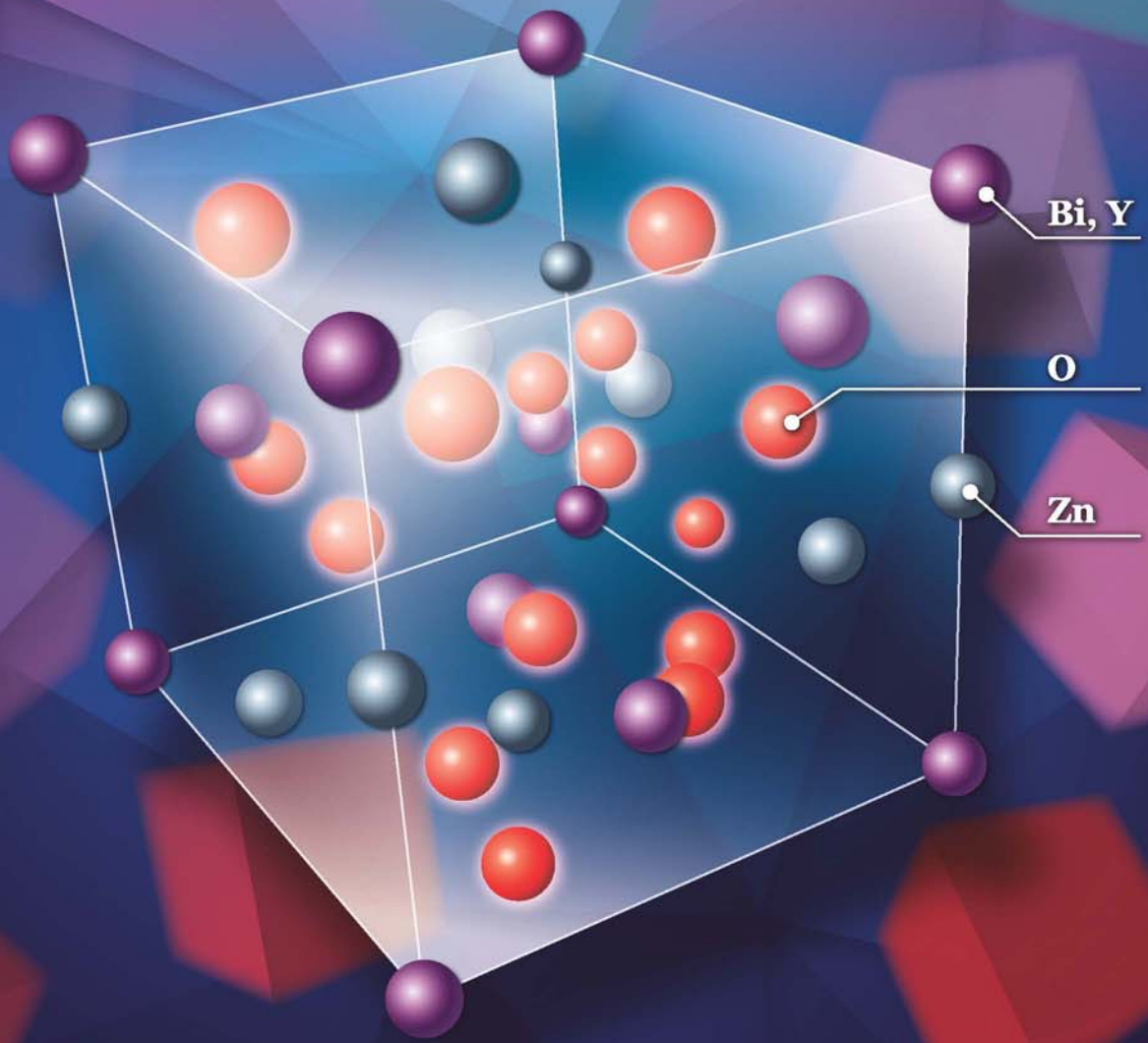

ELSEVIER
Science Press

Sponsored by
Research Center for Eco-Environmental Sciences
Chinese Academy of Sciences

Journal of Environmental Sciences Volume 29 2015

www.jesc.ac.cn

(continued on inside back cover)

CONTENTS

Available online at www.sciencedirect.com

ScienceDirect

www.journals.elsevier.com/journal-of-environmental-sciences

JOURNAL OF ENVIRONMENTAL SCIENCES
www.jesc.ac.cn

Synthesis, crystal structure, photodegradation kinetics and photocatalytic activity of novel photocatalyst $ZnBiYO_4$

*Yanbing Cui, Jingfei Luan**

State Key Laboratory of Pollution Control and Resource Reuse, School of the Environment, Nanjing University, Nanjing 210093, China. E-mail: jfluan@nju.edu.cn

ARTICLE INFO

Article history:
Received 9 April 2014
Revised 13 June 2014
Accepted 17 June 2014
Available online 29 January 2015

Keywords:
$ZnBiYO_4$ and N-doped TiO_2
Methyl orange
Visible light irradiation
Photodegradation pathway
Structural properties

ABSTRACT

$ZnBiYO_4$ was synthesized by a solid-state reaction method for the first time. The structural and photocatalytic properties of $ZnBiYO_4$ were characterized by X-ray diffraction, scanning electron microscopy, X-ray photoelectron spectroscopy and UV–Vis diffuse reflectance. $ZnBiYO_4$ crystallized with a tetragonal spinel structure with space group I41/A. The lattice parameters for $ZnBiYO_4$ were $a = b = 11.176479$ Å and $c = 10.014323$ Å. The band gap of $ZnBiYO_4$ was estimated to be 1.58 eV. The photocatalytic activity of $ZnBiYO_4$ was assessed by photodegradation of methyl orange under visible light irradiation. The results showed that $ZnBiYO_4$ had higher catalytic activity compared with N-doped TiO_2 under the same experimental conditions using visible light irradiation. The photocatalytic degradation of methyl orange with $ZnBiYO_4$ or N-doped TiO_2 as catalyst followed first-order reaction kinetics, and the first-order rate constant was 0.01575 and 0.00416 min^{-1} for $ZnBiYO_4$ and N-doped TiO_2, respectively. After visible light irradiation for 220 min with $ZnBiYO_4$ as catalyst, complete removal and mineralization of methyl orange were observed. The reduction of total organic carbon, formation of inorganic products, SO_4^{2-} and NO_3^-, and evolution of CO_2 revealed the continuous mineralization of methyl orange during the photocatalytic process. The intermediate products were identified using liquid chromatography–mass spectrometry. The $ZnBiYO_4$/(visible light) photocatalysis system was found to be suitable for textile industry wastewater treatment and could be used to solve other environmental chemical pollution problems.

Introduction

Ever since Honda and Fujishima discovered that the photolysis of water could be achieved with a TiO_2 electrode (Fujishima et al., 1979), semiconductor photocatalysts had received more and more attention (Szilágyi et al., 2012; Bi et al., 2011; Zhang et al., 2012). The applications of semiconductor photocatalysts are found mainly in the following fields: (1) photolysis of water to yield hydrogen fuel (Xiang et al., 2012), (2) photodecomposition or photooxidization of hazardous substances (Augugliaro et al., 1999; Ao et al., 2004), (3) photo-induced super-hydrophilicity (Guan, 2005), and (4) artificial photosynthesis (Bard and Fox, 1995). In particular, the photocatalytic decomposition of hazardous substances has been a popular research topic in environmental protection.

TiO_2 has been one of the most widely used and highly efficient semiconductor photocatalysts (Wu et al., 2014; He et al., 2013; Tasbihi et al., 2012). However TiO_2 is only active when irradiated by light with incident wavelength less than 387 nm, and does not respond in the visible light region

* *Corresponding author*. E-mail: jfluan@nju.edu.cn (Jingfei Luan).

http://dx.doi.org/10.1016/j.jes.2014.06.051
1001-0742/

(400 nm < λ < 800 nm). For this reason, the application of TiO_2 has been limited. Therefore, much effort has been devoted to developing visible-light-sensitive photocatalysts, including modification of TiO_2 by doping with elements such as N, C and S (Ren et al., 2007; Giannakas et al., 2013; Selvaraj et al., 2013; Liu and Chen, 2008) or construction of hetero-junctions (Liu et al., 2007; Hou et al., 2007; Elahifard et al., 2007). For instance Zhang utilized N-doped TiO_2 as catalyst to photodegrade phenol under visible light irradiation, and found that the removal ratio of phenol was only 43% after visible light irradiation for 180 min (Zhang et al., 2009). Especially during the last decade, more and more novel photocatalysts have been exploited (Hagiwara et al., 2013; Gamage McEvoy et al., 2013). Spinel-type oxides with a formula of AB_2O_4 such as MIn_2O_4 (M = Ca, Sr, Cd) (Tang et al., 2003; Sato et al., 2001; Sun et al., 2011), $NiCo_2O_4$ (Cui et al., 2009), and $ZnFe_2O_4$/MWCNTs (Chen et al., 2010) have been important compounds, able to decompose methylene blue under visible light irradiation. Furthermore, studies also found that $ZnFe_2O_4$, $CdFe_2O_4$, $ZnBiGaO_4$ and $ZnIn_2S_4$ had good performance in photolysis of organic matter or water photolysis (Xu et al., 2013; Miao et al., 2010; Kale et al., 2010; Wang et al., 2012). The spinel oxide $CdFe_2O_4$ was synthesized by a wet chemical method and was discovered to exhibit catalytic activity in the thermal decomposition of ammonium perchlorate and hydroxyl-terminated polybutadiene (Singh et al., 2010). $ZnFe_2O_4$ also performed well in methyl orange (MO) degradation under xenon lamp irradiation, yielding a maximum degradation ratio of MO of about 37% (Qiu et al., 2004).

In this article, we report a new photocatalyst $ZnBiYO_4$ with a formula of AB_2O_4, which was synthesized by a solid-state reaction method for the first time. $ZnBiYO_4$ seemed likely to have potential for improvement of photocatalytic activity based upon its modified structure, because it has often been found that a slight modification of a semiconductor structure could result in a remarkable change in photocatalytic properties. According to the above analysis, we investigated the photodegradation efficiency of MO by $ZnBiYO_4$ in comparison with N-doped TiO_2. As a result, we found for the first time that $ZnBiYO_4$ showed high activity for degrading an organic dye under visible light irradiation and demonstrated higher activity than N-doped TiO_2. The current investigation provides a simple and easily scaled-up approach to produce photocatalysts for efficient removal of dye effluents in wastewater.

1. Materials and methods

1.1. Synthesis of $ZnBiYO_4$ and N-doped TiO_2

$ZnBiYO_4$ powder was synthesized by a solid-state reaction method. ZnO, Bi_2O_3 and Y_2O_3 with purity of 99.99% were used as raw materials, which were purchased from Sinopharm Group Chemical Reagent Co. (Shanghai, China) and were used without further purification. All powders were dried at 200°C for 4 hr before use. In order to synthesize $ZnBiYO_4$, the precursors were mixed in a quartz mortar, and the mole ratio of ZnO:Bi_2O_3:Y_2O_3 was 2:1:1. Subsequently the precursors were pressed into small cylinders and were placed into an alumina crucible (Shenyang Crucible Corporation, Shenyang, China). Next, the samples were heated at 750°C for 6 hr. Finally, calcination was carried out at 1000°C for 35 hr in an electric furnace (KSL 1700X, Kejing Materials Technology Corporation, Hefei, China). The product was ground in a quartz mortar, producing ultrafine $ZnBiYO_4$ powder. Nitrogen-doped titania (N-doped TiO_2) catalyst was prepared by using a sol–gel method at room temperature. In the procedure, 17 mL tetrabutyl titanate as the titanium precursor and 40 mL absolute ethyl alcohol were fully mixed as solution A, and 40 mL absolute ethyl alcohol, 10 mL glacial acetic acid and 5 mL double distilled water were combined as solution B; then solution A was added dropwise into solution B with vigorous stirring to form a transparent colloidal suspension. Subsequently we added aqueous ammonia into the transparent colloidal suspension with N/Ti proportion of 8 mol% and stirred for 1 hr. Finally, a xerogel was formed after the above mixture was aged for 2 days. Next the xerogel was calcined at 500°C for 2 hr and xerogel powder could be obtained. Subsequently the powder produced was ground in an agate mortar and sieved to obtain N-doped TiO_2 powder.

1.2. Characterization of $ZnBiYO_4$

The phase constitution of $ZnBiYO_4$ was determined by X-ray diffraction (XRD, D/MAX-RB, Rigaku Corporation, Japan) with Cu Kα radiation (λ = 1.54056 Å). The patterns were recorded at 295 K with a step-scan procedure in the range of 2θ = 5°–100°. The step interval was 0.02° and the time per step was 1 sec. Composition of the products was determined using X-ray photoelectron spectroscopy (XPS, ESCALABMK-2, VG Scientific Limited Company, London, U.K.) and a scanning electron microscope coupled with an energy dispersive X-ray spectrometer (EDS, LEO 1530VP, LEO Corporation, Dresden, Germany). At the same time, the content of Zn^{2+}, Bi^{3+}, Y^{3+} and O^{2-} and the valence state of elements were also analyzed by XPS. UV–visible diffuse reflectance spectra were measured using a UV–Vis spectrophotometer (Shimadzu UV-2550, Shimadzu Corporation, Kyoto, Japan) and $BaSO_4$ was used as the reference material.

1.3. Photocatalytic activity tests

The photocatalytic activity of $ZnBiYO_4$ powder was evaluated by photodegradation of methyl orange aqueous solution ($C_{14}H_{14}N_3NaO_3S$). The photoreaction was carried out in a photocatalytic reactor as shown in Fig. 1. It consists of three parts: reactor, high pressure xenon lamp and Cooling System (Xujiang Machine Plant, Nanjing, China). The internal structure of the reaction apparatus was as follows: the lamp was surrounded by a quartz sheath with a hollow structure and was located in the middle of the reactor. Twelve holes were used to fix quartz tubes, which were evenly distributed around the lamp, and the photocatalytic reaction took place in these quartz tubes. Between the xenon lamp and quartz tubes, optical filters were used to obtain light of different wavelengths. In the experiment involving photocatalytic degradation of MO, UV-CUT420 filters were used to obtain light with wavelength more than 420 nm. In the experiment testing photonic efficiency, band pass filters were used to obtain light of different single wavelengths such as 400, 420, 450, 500, 530, 560, 600, 650, 700 and 750 nm (Nantong GuoGuang Optical Glass, China). The cooling water through

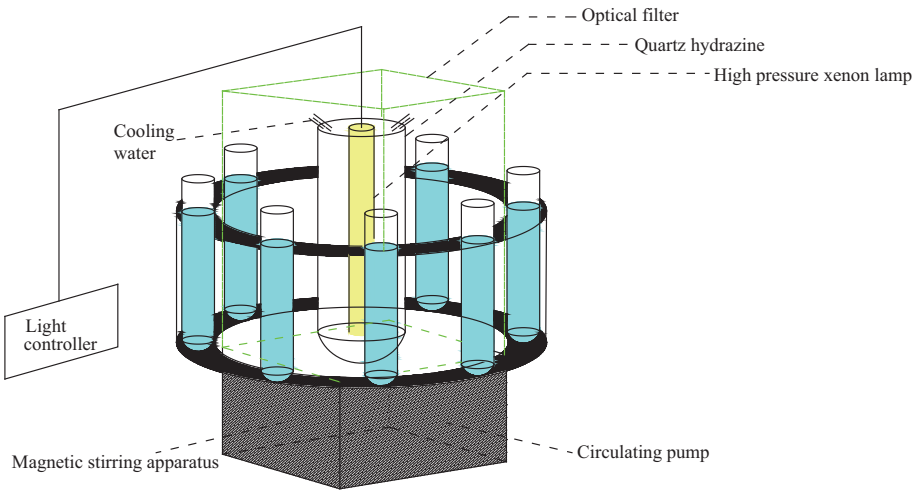

Fig. 1 – Schematic plot of the photocatalytic reaction instrument.

the reactor maintained a near constant reaction temperature (20°C) and the reaction solution was stirred and aerated continuously. Under magnetic stirring, the photocatalyst powder was kept in suspension in the MO solution. In this study, 0.30 g $ZnBiYO_4$ powder was added into a quartz tube containing 300 mL of 0.030 mmol MO aqueous solution. The visible light source was a 500 W Xenon lamp. Prior to visible light irradiation, the suspensions containing the catalyst and MO dye were magnetically stirred in the dark for 45 min to ensure establishment of an adsorption/desorption equilibrium among $ZnBiYO_4$, the MO dye and atmospheric oxygen. When the reactor was irradiated to induce the photocatalytic decomposition reaction, the suspension was stirred at 500 r/min, the initial pH of the MO solution was 7.0 and the temperature of the reaction suspension was kept at 20 ± 2°C. During the reaction, quartz tubes were taken out from the reactor at various time intervals and the suspension was filtered through 0.22 μm membrane filters. Next, the filtrate was analyzed by a Shimadzu UV-2550 UV–Visible spectrometer (Shimadzu Corporation, Kyoto, Japan) with the detecting wavelength at 465 nm. The experimental error was found to be within ±2.2%.

The inorganic products obtained from MO degradation were analyzed by ion chromatography (DX-300, Dionex Corporation, Sunnyvale, USA). The identification and measurement of MO and its intermediate degradation products were carried out by liquid chromatography–mass spectrometry (LC-MS, Thermo Quest LCQ Duo, Thermo Fisher Scientific Corporation, Massachusetts, USA. Beta Basic-C18 HPLC column: 150 × 2.1 mm, ID of 5 μm, Thermo Fisher Scientific Corporation, Massachusetts, USA.). Here, 20 μL of solution obtained after the photocatalytic reaction was injected automatically into the LC–MS system. The mobile phase contained 60% methanol and 40% water, and the flow rate was 0.2 mL/min. MS conditions included an electrospray ionization interface, capillary temperature of 27°C with a voltage of 19.00 V, spray voltage of 5000 V and a constant sheath gas flow rate. The spectrum was acquired in the negative ion scan mode and the *m*/*z* range swept from 50 to 600. Evolution of CO_2 was analyzed with an Intersmat™ IGC120-MB gas chromatograph (Thermo Separation Products Corporation, Brussels, Belgium) equipped with a Porapack Q column (3 m in length and 0.25 m in inner diameter), which was connected to a catharometer detector (Thermo Separation Products Corporation, Antwerpen, Belgium). The total organic carbon (TOC) concentration was determined with a TOC analyzer (TOC-5000, Shimadzu Corporation, Kyoto, Japan). The incident photon flux I_o, which was measured by a radiometer (FZ-A radiometer, Photoelectric Instrument Factory Beijing Normal University, Beijing, China), was determined to be 4.76×10^{-6} Einstein L^{-1} sec^{-1} under visible light irradiation (wavelength range of 400–700 nm). The incident photon flux on the photoreactor was varied by adjusting the distance between the photoreactor and the Xe arc lamp. The photonic efficiency was calculated according to the following equation (Marugán et al., 2006; Sakthivel et al., 2004):

$$\varphi = R/I_o \quad (1)$$

where, φ is the photonic efficiency (%), R is the rate of MO degradation (mol/(L·sec)), and I_o is the incident photon flux (Einstein L^{-1} sec^{-1}).

2. Results and discussion

2.1. SEM-EDS and XRD analysis of $ZnBiYO_4$

The morphology of as-prepared $ZnBiYO_4$ was investigated by SEM. Fig. 2a presents the SEM image of $ZnBiYO_4$. It can be seen clearly from Fig. 2a that the morphology of the $ZnBiYO_4$ particles was very uniform and regular. The average particle size of $ZnBiYO_4$ was about 2.0 μm. Moreover, Fig. 2b shows enlarged SEM images of $ZnBiYO_4$. It can be seen from Fig. 2b that the $ZnBiYO_4$ particles crystallized well and the surface of the $ZnBiYO_4$ particle was composed of different crystal faces. Fig. 3 shows the SEM-EDS spectrum of $ZnBiYO_4$, which gives further support to the above results. As illustrated in Fig. 3, we could find that $ZnBiYO_4$ was a pure phase without any observed impurities, and $ZnBiYO_4$ showed the presence of zinc, bismuth, yttrium and oxygen elements.

To obtain information about the phase structure and purity of the as-prepared sample, $ZnBiYO_4$ was characterized by X-ray diffraction (XRD). Fig. 4a shows the experimental

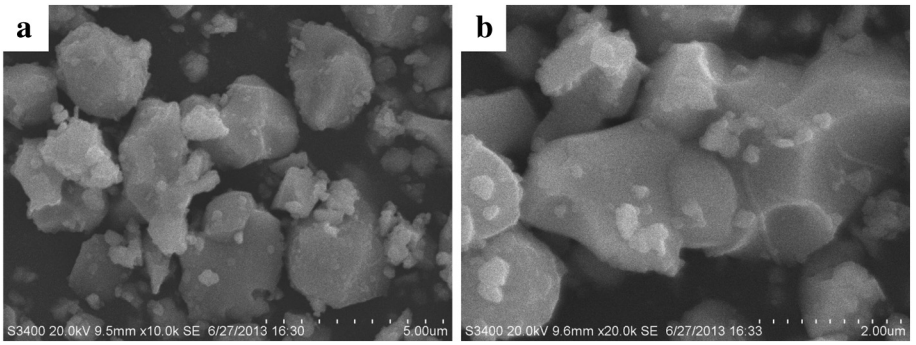

Fig. 2 – Scanning electron microscopy (SEM) (a) and enlarged (b) SEM image of the $ZnBiYO_4$ photocatalyst.

XRD pattern and the corresponding Rietveld refinement result for $ZnBiYO_4$. The strong and sharp diffraction peaks indicated the highly perfect crystallinity of $ZnBiYO_4$. Rietveld analysis was performed to ensure the phase purity of $ZnBiYO_4$ and obtain detailed crystal structure information. Full-profile structure refinements of the collected X-ray diffraction data of $ZnBiYO_4$ were obtained using the RIETAN™ program, which was based on Pawley analysis. Many parameters were iteratively refined, such as zero shifts, scale factors, background, lattice, line, atomic positions, site occupations, and so on. An acceptable reliability factor of R = 9.68% was obtained. Based on the high purity of the raw materials and the EDS results that did not detect any other elements, it was not plausible that the slightly high R factor was caused by the presence of impurities. Therefore, it was concluded that the slightly high R factor for $ZnBiYO_4$ was due to a slightly modified structure of $ZnBiYO_4$ compared with $CdFe_2O_4$. The lattice parameter of $CdFe_2O_4$ crystal with a cubic structure (a = 8.698 Å) changed when Fe^{3+} was replaced by Bi^{3+} and Y^{3+}, because the Y^{3+} ionic radius (1.019 Å) and Bi^{3+} ionic radius (1.17 Å) were larger than the Fe^{3+} ionic radius (0.78 Å). The results of the final refinement for $ZnBiYO_4$ indicated good agreement between the observed and calculated data in a tetragonal spinel structure with space group I41/A, $a = b$ = 11.176 Å and c = 10.014 Å.

The atomic coordinates and structural parameters of $ZnBiYO_4$ are listed in Table 1. Combining the refinement results, the structure of $ZnBiYO_4$ was depicted as shown in Fig. 4b, which clearly shows that $ZnBiYO_4$ has a typical spinel structure.

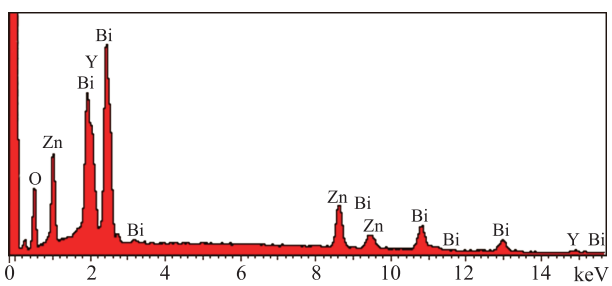

Fig. 3 – Selected area energy diffraction spectrum pattern (EDS) of $ZnBiYO_4$.

2.2. XPS analysis of $ZnBiYO_4$

The X-ray photoelectron spectrum of $ZnBiYO_4$ was measured to investigate the surface chemical composition and valence state of Zn, Bi, Y and O. Fig. 5 shows the full XPS spectrum of $ZnBiYO_4$. Fig. 5 indicates that the main peaks were due to the elements of Zn, Bi, Y and O. Meanwhile, the detailed XPS spectra of $Zn2p_{3/2}$, $Bi4f_{7/2}$,$Y3d_{5/2}$ and O1s are shown in Fig. 6. The binding energies of the elements of $ZnBiYO_4$ confirmed that the valences of Zn, Bi, Y and O were +2, +3, +3 and −2. Furthermore, the average atomic ratio of Zn:Bi:Y:O for $ZnBiYO_4$ was 1.00:0.96:1.02:3.97 based on XPS results and SEM-EDS results. These results suggested that the raw materials were highly pure and the prepared sample was composed of single-phase $ZnBiYO_4$.

2.3. UV–Vis analysis of $ZnBiYO_4$ and N-doped TiO_2

In order to study the optical response of $ZnBiYO_4$ nanoparticles, the UV–Vis diffuse reflectance spectra were measured. Fig. 7a represents the absorption spectrum of $ZnBiYO_4$. A broad absorbance shoulder from 550 to 700 nm was clearly observed, which indicated that $ZnBiYO_4$ had the ability to respond to visible light. Compared with the spectrum of N-doped TiO_2 as shown in Fig. 7b, clearly $ZnBiYO_4$ had higher response to visible light. The insets within Fig. 7 show that the values of band gap Eg for $ZnBiYO_4$ and N-doped TiO_2 were 1.58 and 2.76 eV, which were calculated based on the equation (Zou et al., 2000).

$$\alpha h\nu = A(h\nu - E_g)^n \quad (2)$$

where, E_g and n could be calculated by the following steps: (1) plotting $\ln(\acute{a}h\nu)$ *versus* $\ln(h\nu - E_g)$ by assuming an approximate value of E_g, (2) deducing the value of n according to the slope of this graph, (iii) refining the value of E_g by plotting $(\acute{a}h\nu)^{1/n}$ *versus* $h\nu$ and extrapolating the plot to the point of $(\acute{a}h\nu)^{1/n} = 0$. According to the above analysis, the light absorbance of the $ZnBiYO_4$ sample in the visible light region was of great importance for its practical application because it could be activated by sunlight. The narrow band gap of the $ZnBiYO_4$ sample further indicated that it could absorb most of the visible light spectrum.

2.4. Photodegradation of MO with $ZnBiYO_4$ and N-doped TiO_2 as catalyst

The photocatalytic activities of $ZnBiYO_4$ powder and N-doped TiO_2 powder were evaluated and compared by decomposition

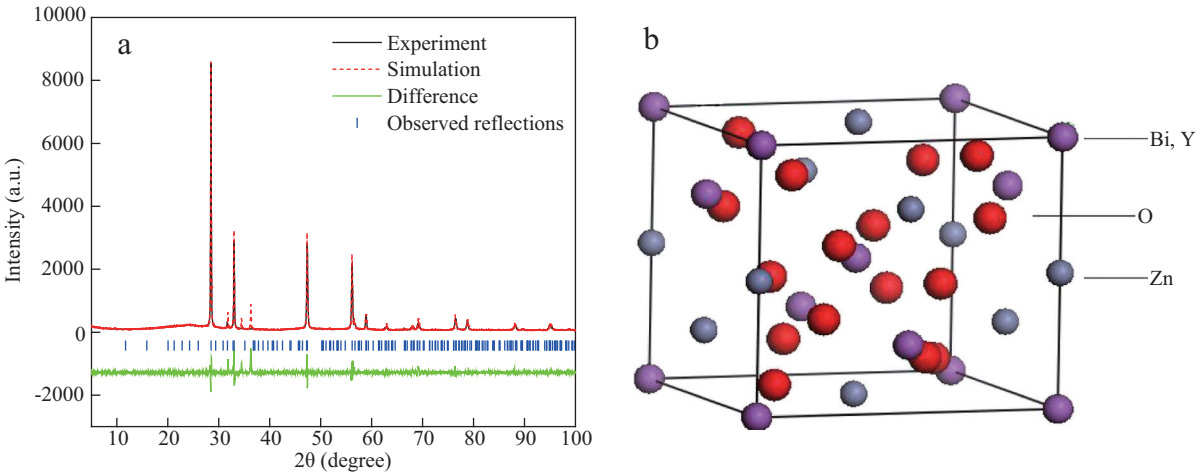

Fig. 4 – Experimental X-ray diffraction (XRD) pattern (a) and the corresponding Rietveld refinement result of $ZnBiYO_4$ (b) the structure of $ZnBiYO_4$.

of MO in aqueous solution under visible light irradiation. Fig. 8 shows the UV–Vis spectra of the methyl orange in different conditions. The maximum absorption wavelength of MO was 468.2 nm. According to Fig. 8, we can see that when MO was irradiated by visible light for 220 min without photocatalyst, almost no photodegradation of MO occurred. Compared with $ZnBiYO_4$, N-doped TiO_2 had a greater adsorption capacity when stirred with MO in the dark for 220 min, but both materials had weak adsorption capacity toward MO. Thus, we inferred that the degradation of MO was caused by photocatalysis, rather than being caused by adsorption and photolysis. Fig. 9 shows the temporal evolution of the concentration of MO under visible light irradiation ($\lambda > 420$ nm) in the presence of $ZnBiYO_4$ or N-doped TiO_2 as well as in the absence of a photocatalyst. The results showed that $ZnBiYO_4$ indeed could promote the photodegradation efficiency of MO under visible light irradiation. Besides, the photodegradation removal rate of MO in the presence of $ZnBiYO_4$ was 2.150×10^{-9} mol/(L·sec), which was faster than the photodegradation removal rate of 1.230×10^{-9} mol/(L·min) in the presence of N-doped TiO_2. The photonic efficiency of $ZnBiYO_4$ was estimated to be 0.0452% ($\lambda = 420$ nm) while that of N-doped TiO_2 was 0.0258% ($\lambda = 420$ nm). The photodegradation removal rate of MO was 7.85% after visible light irradiation for 220 min in the absence of a photocatalyst. However, in the presence of $ZnBiYO_4$ or N-doped TiO_2, the photodegradation removal rate was 96.88% and 55.43% respectively. By comparison, we could clearly find that $ZnBiYO_4$ possessed higher photocatalytic activity than N-doped TiO_2, which might be caused by its high quantum efficiency.

Fig. 10a shows the change of TOC during the photocatalytic degradation of MO with $ZnBiYO_4$ or N-doped TiO_2 as catalyst under visible light irradiation. The TOC measurements revealed the disappearance of organic carbon in the MO solutions. The results showed that 95.07% or 53.37% of TOC decrease was obtained after visible light irradiation for 220 min when $ZnBiYO_4$ or N-doped TiO_2 was utilized as photocatalyst. Therefore, the above results indicated that MO was almost completely mineralized by $ZnBiYO_4$. Fig. 10b shows the amount of CO_2 yielded during the process of decomposing MO with $ZnBiYO_4$ or N-doped TiO_2 as catalyst under visible light irradiation. The amount of CO_2 increased gradually with increasing reaction time when MO was photodegraded with $ZnBiYO_4$ or N-doped TiO_2 as catalyst. At the same time, after visible light irradiation of 220 min, the CO_2 production of 0.117 mmol with $ZnBiYO_4$ as catalyst was higher than the CO_2 production of 0.0654 mmol with N-doped TiO_2.

Table 1 – The atomic coordinates within the cell and lattice parameters of $ZnBiYO_4$.

Atom	x	y	z	Occupation factor
Zn	0	0	0.5	1
Bi	0	0	0	1
Y	0	0	0	1
O	0.767	0.140	0.0819	1
Lattice parameters		$a = b = 11.176$ Å $c = 10.0143$ Å $\alpha = \beta = \gamma = 90°$ Tetragonal system, space group I41/A		

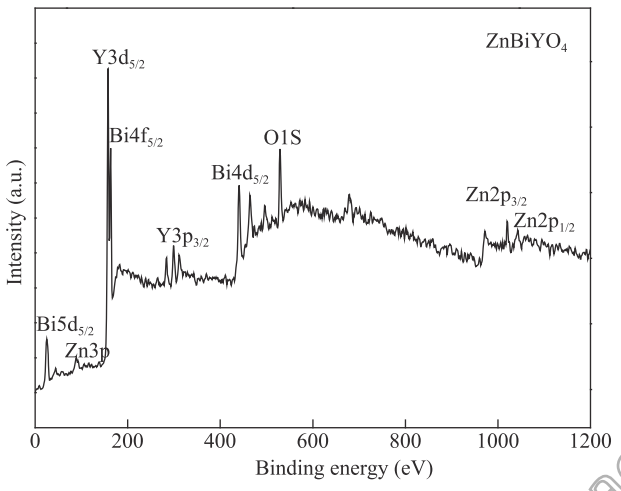

Fig. 5 – Full X-ray photoelectron spectrum of $ZnBiYO_4$.

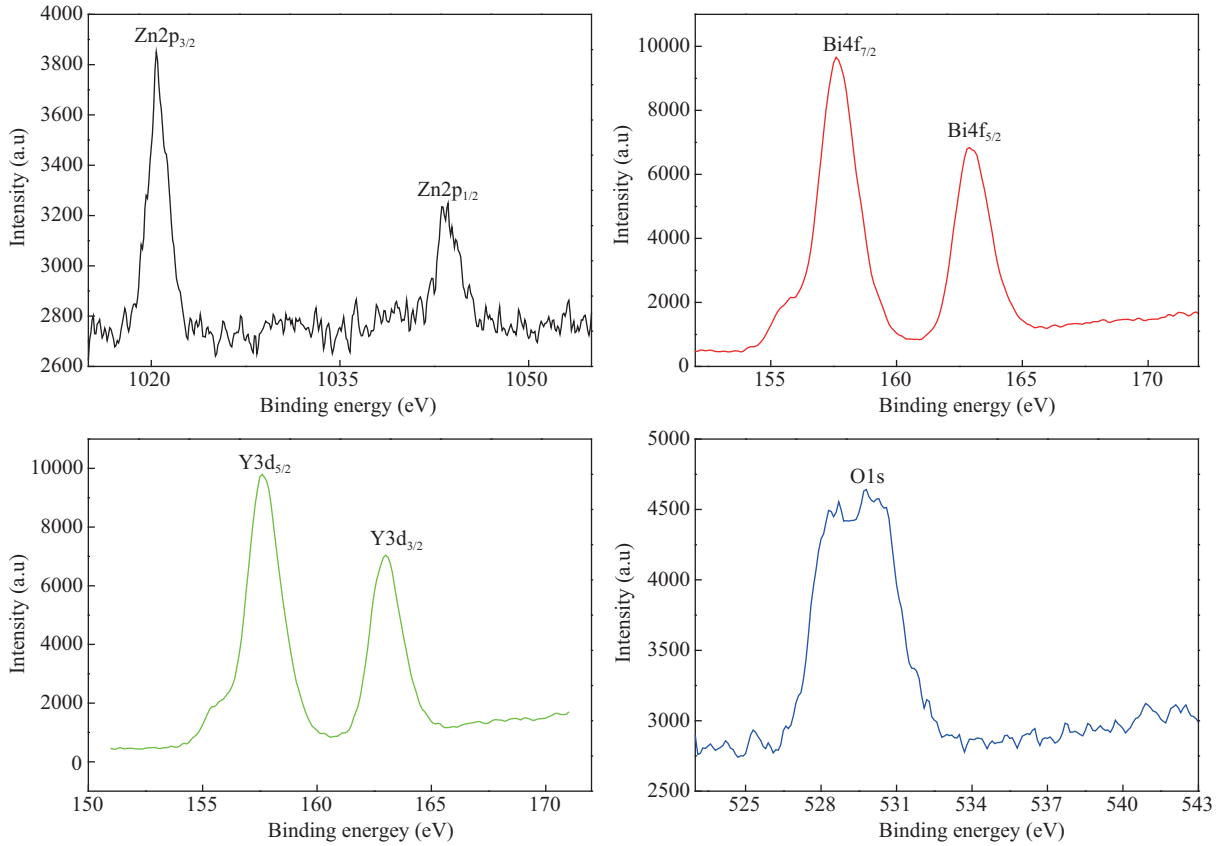

Fig. 6 – The detailed X-ray photoelectron spectroscopy (XPS) spectra of Zn2p, Bi4f, Y3d and O1s.

The first-order nature of the photocatalytic degradation kinetics with $ZnBiYO_4$ or N-doped TiO_2 as catalyst is clearly demonstrated in Fig. 11. The results showed a linear correlation between $\ln(C/C_o)$ (or $\ln(TOC/TOC_o)$) and the irradiation time for the photocatalytic degradation of MO under visible light irradiation in the presence of $ZnBiYO_4$ or N-doped TiO_2. According to Fig. 11a, the first-order rate constant k_C of MO concentration was estimated to be 0.0158 min^{-1} with $ZnBiYO_4$ as catalyst and 0.00416 min^{-1} with N-doped TiO_2. The different values of k_C indicated that $ZnBiYO_4$ was more suitable for the photocatalytic degradation of MO under visible light irradiation than N-doped TiO_2. According to the data from Fig. 11b, the first-order rate constant K_{TOC} of TOC removal was estimated to be 0.0125 min^{-1} with $ZnBiYO_4$ as catalyst and 0.00357 min^{-1} with N-doped TiO_2. The different values between k_C and K_{TOC} indicated that intermediate photodegradation products of MO probably appeared during the photocatalytic degradation process.

Fig. 12 shows the concentration variation of NO_3^- and SO_4^{2-} during the photocatalytic degradation process of MO with

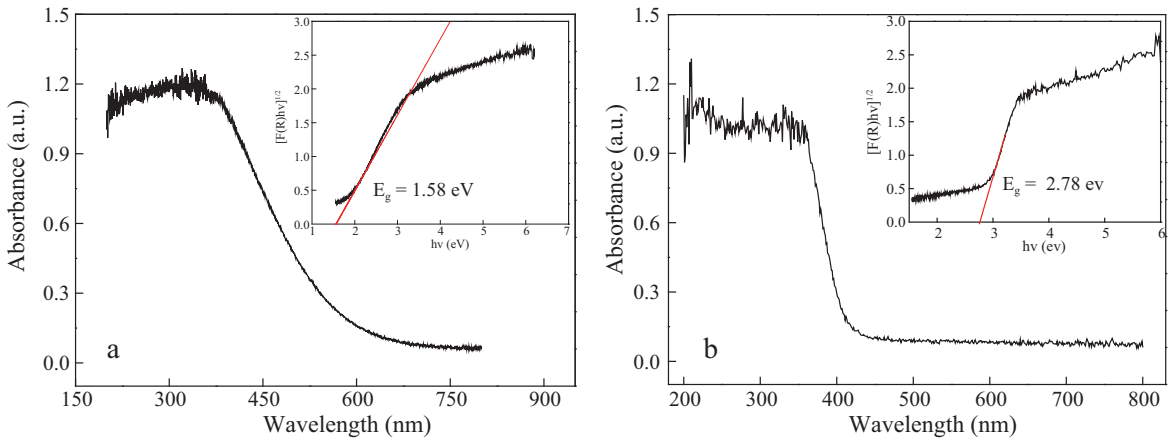

Fig. 7 – The UV-Vis diffuse reflectance spectrum of $ZnBiYO_4$ (a) and N-doped TiO^2 (b). The inset shows the value of band gap Eg of $ZnBiYO_4$ for (a) and N-doped TiO_2 for (b).

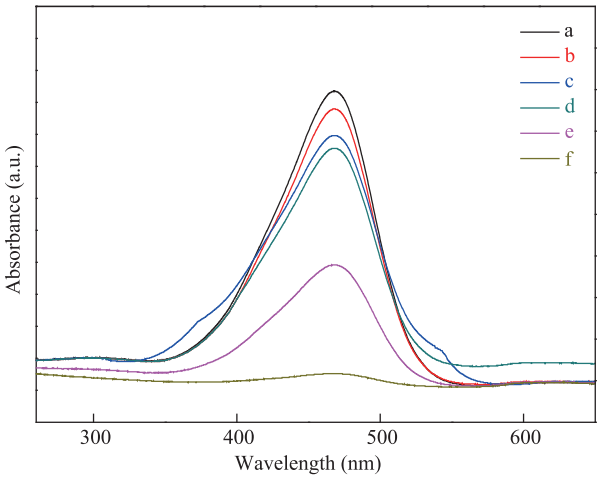

Fig. 8 – UV–Vis spectra of the MO. (a) original methyl orange (MO); (b) MO solution only irradiated by visible light without photocatalyst for 220 min; (c) MO solution with $ZnBiYO_4$ in the dark for 220 min; (d) MO solution with N-doped TiO_2 in the dark for 220 min; (e) MO solution with $ZnBiYO_4$ under the visible light for 220 min; (f) MO solution with N-doped TiO_2 under the visible light for 220 min.

$ZnBiYO_4$ or N-doped TiO_2 as catalyst under visible light irradiation. Fig. 12a shows that the NO_3^- ion concentration was 0.0616 or 0.0487 mmol and the theoretical stoichiometric amount of NO_3^- ion was 0.027 mmol, indicating that 68.47% or 53.33% of nitrogen from MO was converted into nitrate ions. According to Fig. 12b, the SO_4^{2-} ion concentration was 0.0192 or 0.0137 mmol and the theoretical stoichiometric amount of SO_4^{2-} ion was 0.009 mmol, indicating that 64.07% or 45.63% of sulfur from MO was converted into sulfate ions. Compared with the theoretical stoichiometric amount of NO_3^- and SO_4^{2-}, the amount of SO_4^{2-} ions and NO_3^- ions released into the solution attracted our attention. It was found that both the SO_4^{2-} ion concentration and NO_3^- ion concentration were lower than the theoretical stoichiometric amount based on the MO concentration. One possible reason could be a loss of volatile compounds such as SO_2, NH_3, and N_2 (Konstantinou and Albanis, 2004). The second reason was probably the formation of other water-soluble ions such as SO_3^{2-} and NH_4^+. The most likely reason might come from partially irreversible adsorption of some SO_4^{2-} and NO_3^- ions on the surface of the photocatalyst, which had been observed by Lachheb et al. (2002) with titanium dioxide as catalyst. No matter whether the sulfate ions or nitrate ions were adsorbed on the surface of the photocatalyst or not, the above results indicated that the photocatalytic activity of $ZnBiYO_4$ was not restrained.

In order to investigate the degradation pathway of MO, LC–MS was utilized to assess the degradation products of MO. Fig. 13 shows the corresponding mass spectra of a MO solution that was irradiated for 50 min, at different retention times of 2.2, 4.0 and 6.9 min. Intermediate products from the photodegradation process of MO with different *m*/z values (191, 290 and 304) were confirmed, with the peak of *m*/z = 191 appearing at 2.2 min, that of *m*/z = 291 at 4.0 min, and that of *m*/z = 304 at 6.9 min. The mass to charge ratio of MO was verified to be *m*/z = 304. The intermediate products were identified as 1,3-dyhydroxy-benzene sulfonic acid (*m*/z = 191) and 4-[4-(methylamino)phenylazo] benzenesulfonate (*m*/z = 291). Based on the above results, a possible photocatalytic degradation pathway for MO was proposed. The molecule of MO was converted to small organic species, which were subsequently mineralized into inorganic products such as SO_4^{2-} ions, NO_3^- ions, CO_2 and water ultimately.

To evaluate the utilization percent of visible light, a photonic efficiency experiment was carried out. Fig. 14 shows the photonic efficiency of $ZnBiYO_4$ and N-doped TiO_2 during irradiation of MO at different incident wavelengths from 400 to 700 nm. $ZnBiYO_4$ was more efficient than N-doped TiO_2 in the process of photocatalysis of MO. For incident wavelengths more than 550 nm, photonic efficiency showed almost no change. The

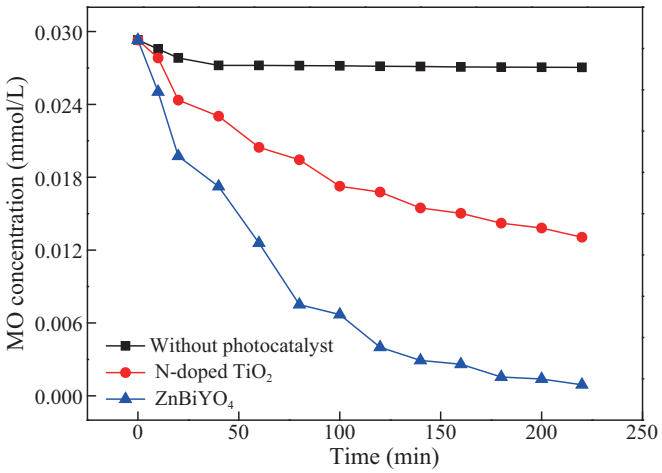

Fig. 9 – Temporal evolution of methyl orange (MO) concentration under visible light irradiation in the presence of $ZnBiYO_4$, N-doped TiO_2 as well as in the absence of a photocatalyst.

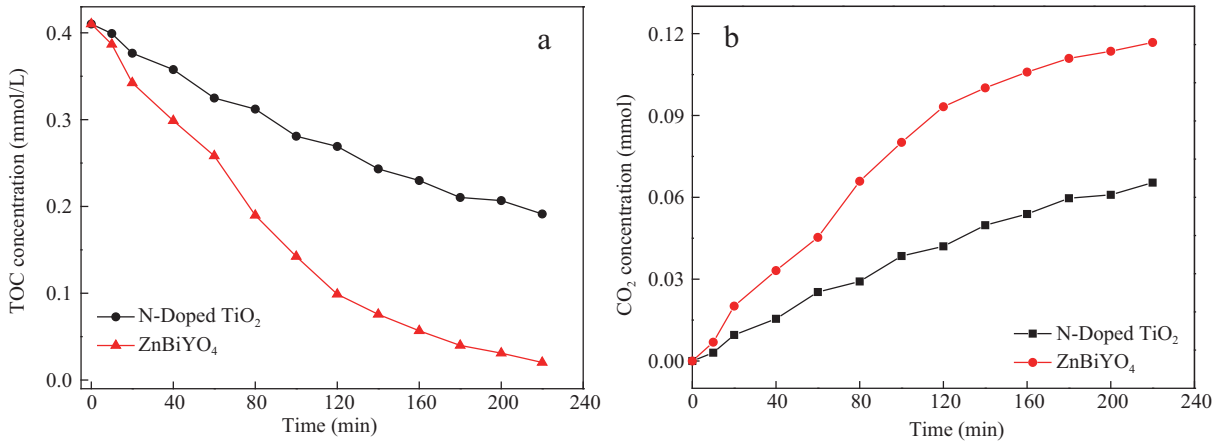

Fig. 10 – (a) The change of total organic carbon (TOC) during photocatalytic degradation of methyl orange (MO) with $ZnBiYO_4$ or N-doped TiO_2 as catalyst under visible light irradiation, (b) the amount of CO_2.

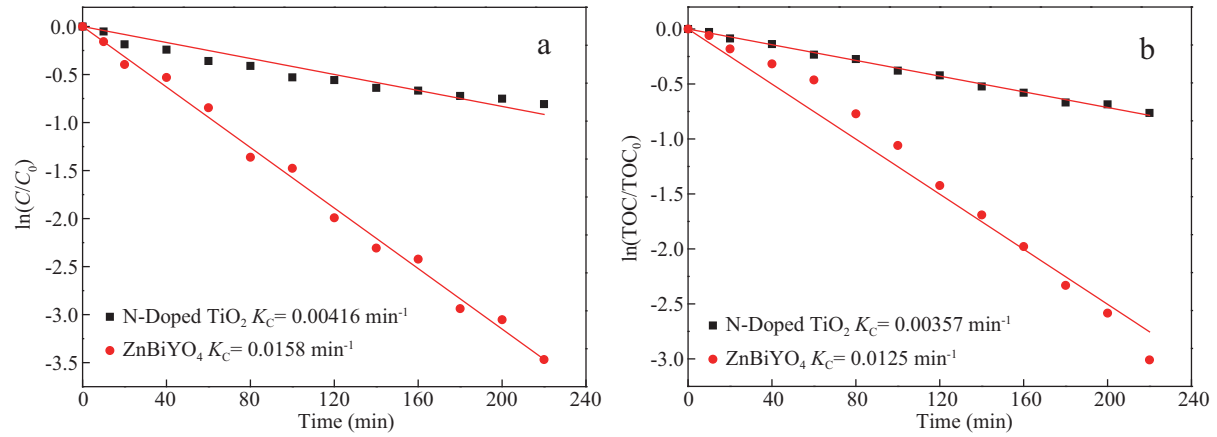

Fig. 11 – The first-order nature of the photocatalytic degradation kinetics with $ZnBiYO_4$ or N-doped TiO_2 as catalyst. (a) $\ln(C/C_0)$ *versus* irradiation time and (b) $\ln(TOC/TOC_0)$ *versus* irradiation time.

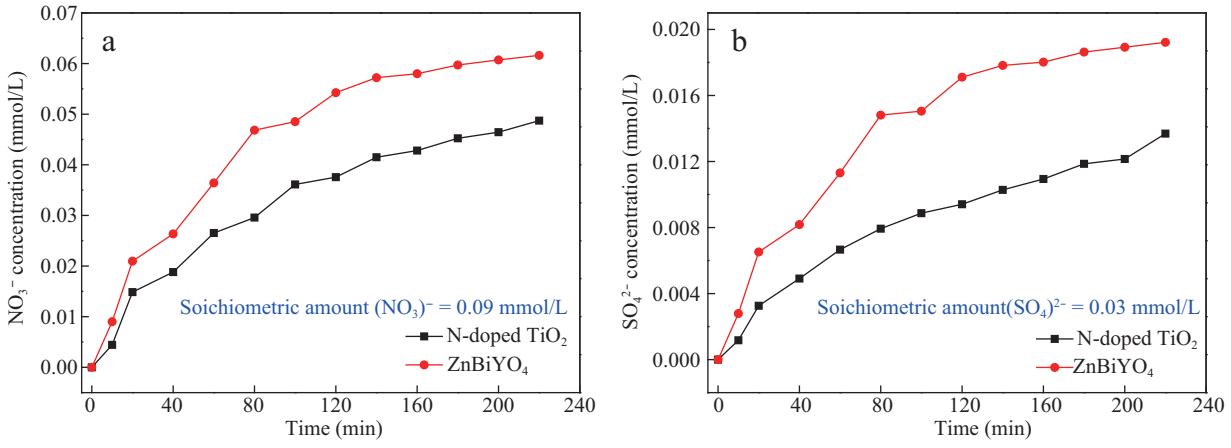

Fig. 12 – Concentration variation of NO_3^- ions and SO_4^{2-} ions during photocatalytic degradation of methyl orange (MO) with $ZnBiYO_4$ or N-doped TiO_2 as catalyst and the theoretical stoichiometric amount of NO_3^- ions and SO_4^{2-} ions.

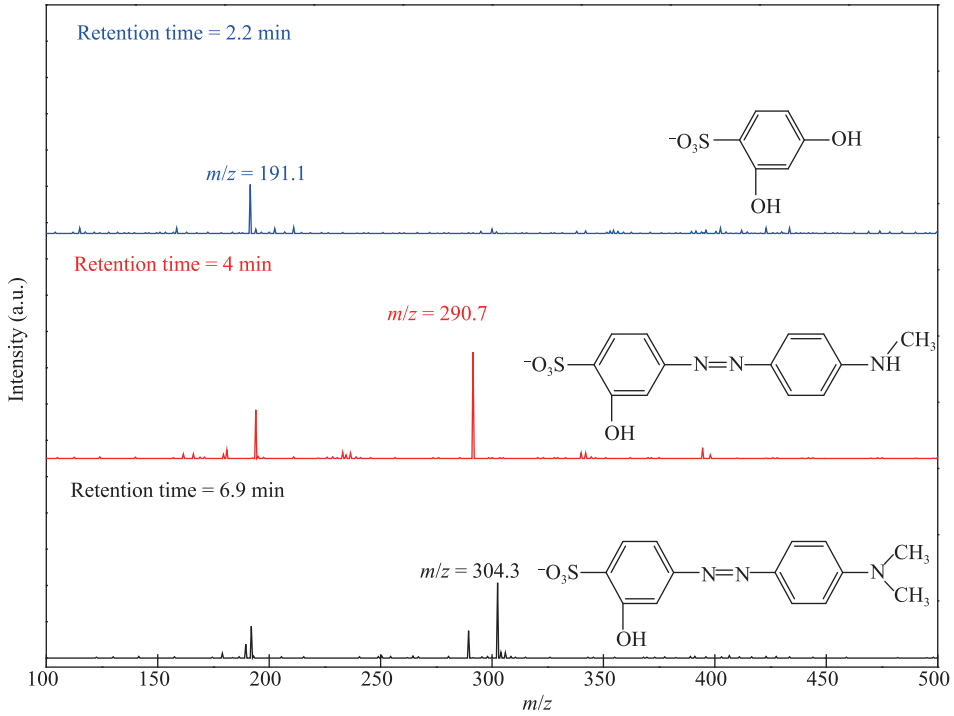

Fig. 13 – Mass spectrum of methyl orange (MO) solution irradiated 50 min at different retention time of 2.25, 4.05, and 6.90 min.

photonic efficiency of $ZnBiYO_4$ when irradiating MO at different incident wavelengths was in accordance with its band structure. These results provided evidence that $ZnBiYO_4$ produced electron–hole pairs by absorption of photons directly.

The present results indicated that the $ZnBiYO_4$–visible light photocatalysis system might be regarded as a practical method for treatment of diluted colored wastewater. This system could be used for decolorization, purification and detoxification of wastewater from textile, printing and dyeing industries in the long-day countries. Meanwhile, this system did not need high pressure oxygen, heating or any chemical reagents. A large amount of decolorized and detoxified water was produced through treatment by our new system, and the results showed that the $ZnBiYO_4$–visible light photocatalysis system might provide a valuable treatment for purifying and reusing colored aqueous effluents.

3. Conclusions

$ZnBiYO_4$ was prepared by a solid-state reaction method for the first time. The structural and photocatalytic properties of $ZnBiYO_4$ were investigated. XRD results indicated that $ZnBiYO_4$ crystallized in the tetragonal spinel structure with space group I41/A. The lattice parameters of $ZnBiYO_4$ were found to be a = b = 11.176 Å and c = 10.014 Å. The band gap of $ZnBiYO_4$ was estimated to be about 1.58 eV, suggesting that $ZnBiYO_4$ possessed optical absorption ability in the visible light region. Photocatalytic

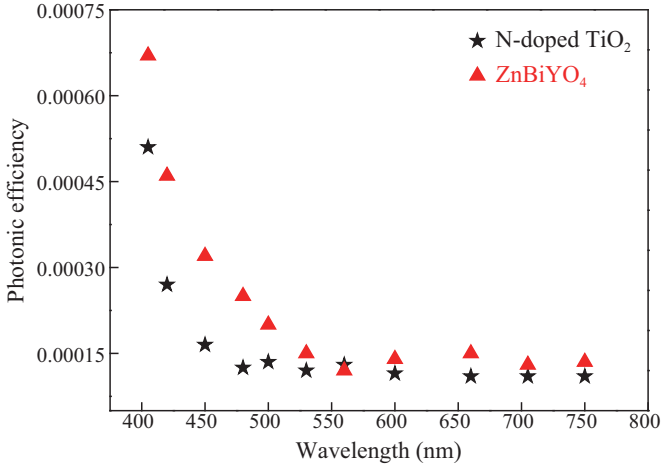

Fig. 14 – Photonic efficiency of $ZnBiYO_4$ and N-doped TiO_2 at different incident wavelengths.

decomposition of aqueous MO was realized under visible light irradiation with $ZnBiYO_4$ or N-doped TiO_2 as catalyst. The results showed that $ZnBiYO_4$ possessed higher photocatalytic activity compared with N-doped TiO_2 for photocatalytic degradation of MO under visible light irradiation. The photocatalytic degradation of MO with $ZnBiYO_4$ or N-doped TiO_2 as catalyst followed first-order reaction kinetics. The apparent first-order rate constant of $ZnBiYO_4$ or N-doped was 0.0158 or 0.00416 min^{-1}. Complete removal and mineralization of MO were observed after visible light irradiation for 220 min with $ZnBiYO_4$ as catalyst. The reduction of total organic carbon, formation of inorganic products such as SO_4^{2-} and NO_3^-, and the evolution of CO_2 revealed the continuous mineralization of MO during the photocatalytic process. Using the LC–MS technique, intermediate products were identified. The $ZnBiYO_4$/(visible light) photocatalysis system was found to have potential for textile industry wastewater treatment and could be used to solve other environmental chemical pollution problems.

Acknowledgments

This work was supported by the National Natural Science Foundation of China (No. 21277067), and grants from the China-Israel Joint Research Program in Water Technology and Renewable Energy (No. 5), Natural Science Foundation of Jiangsu Province (No. BK20141312), and the Project of Science and Technology Development Plan of Suzhou City of China from 2014 (No. ZXG201440).

REFERENCES

Ao, C.H., Lee, S.C., Zou, S.C., Mak, C.L., 2004. Inhibition effect of SO_2 on NOx and VOCs during the photodegradation of synchronous indoor air pollutants at parts per billion (ppb) level by TiO_2. Appl. Catal. B 49 (3), 187–193.

Augugliaro, V., Coluccia, S., Loddo, V., Marchese, L., Martra, G., Palmisano, L., et al., 1999. Photocatalytic oxidation of gaseous toluene on anatase TiO_2 catalyst: mechanistic aspects and FT-IR investigation. Appl. Catal. B 20 (1), 15–27.

Bard, A.J., Fox, M.A., 1995. Artificial photosynthesis-solar splitting of water to hydrogen and oxygen. Acc. Chem. Res. 28 (3), 141–145.

Bi, Y.P., Ouyang, S.X., Umezawa, N., Cao, J.Y., Ye, J.H., 2011. Facet effect of single-crystalline Ag_3PO_4 sub-microcrystals on photocatalytic properties. J. Am. Chem. Soc. 133 (17), 6490–6492.

Chen, C.H., Liang, Y.H., Zhang, W.D., 2010. $ZnFe_2O_4$/MWCNTs composite with enhanced photocatalytic activity under visible-light irradiation. J. Alloys Compd. 501 (1), 168–172.

Cui, B., Lin, H., Li, Y.Z., Li, J.B., Sun, P., Zhao, X.C., et al., 2009. Photophysical and photocatalytic properties of core-ring structured $NiCo_2O_4$ nanoplatelets. J. Phys. Chem. C 113 (32), 14083–14087.

Elahifard, M.R., Rahimnejad, S., Haghighi, S., Gholami, M.R., 2007. Apatite-coated Ag/AgBr/TiO_2 visible-light photocatalyst for destruction of bacteria. J. Am. Chem. Soc. 129 (31), 9552–9553.

Fujishima, A., Inoue, T., Honda, K., 1979. Competitive photoelectrochemical oxidation of reducing agents at the TiO_2 photoanode. J. Am. Chem. Soc. 101 (19), 5582–5588.

Gamage McEvoy, J., Bilodeau, D.A., Cui, W.Q., Zhang, Z.S., 2013. Visible-light-driven inactivation of *Escherichia coli* K-12 using an Ag/AgCl-activated carbon composite photocatalyst. J. Photochem. Photobiol. A 267, 25–34.

Giannakas, A.E., Seristatidou, E., Deligiannakis, Y., Konstantinou, I., 2013. Photocatalytic activity of N-doped and N-F co-doped TiO_2 and reduction of chromium(VI) in aqueous solution: an EPR study. Appl. Catal. B 132, 460–468.

Guan, K.H., 2005. Relationship between photocatalytic activity, hydrophilicity and self-cleaning effect of TiO_2/SiO_2 films. Surf. Coat. Technol. 191 (2–3), 155–160.

Hagiwara, H., Nagatomo, M., Seto, C., Ida, S., Ishihara, T., 2013. Dye-modification effects on water splitting activity of GaN: ZnO photocatalyst. J. Photochem. Photobiol. A 272, 41–48.

He, Z.Q., Cai, Q.L., Fang, H.Y., Situ, G., Qiu, J.P., Song, S., et al., 2013. Photocatalytic activity of TiO_2 containing anatase nanoparticles and rutile nanoflower structure consisting of nanorods. J. Environ. Sci. 25 (12), 2460–2468.

Hou, L.-R., Yuan, C.-Z., Peng, Y., 2007. Synthesis and photocatalytic property of SnO_2/TiO_2 nanotubes composites. J. Hazard. Mater. 139 (2), 310–315.

Kale, B.B., Baeg, J.O., Kong, K.J., Moon, S.J., Lee, S.M., So, W.W., 2010. Synthesis and structural analysis of visible light photocatalyst, $ZnBiGaO_4$ for photocatalytic solar hydrogen production. Int. J. Energy Res. 34 (5), 404–411.

Konstantinou, I.K., Albanis, T.A., 2004. TiO_2-assisted photocatalytic degradation of azo dyes in aqueous solution: kinetic and mechanistic investigations: a review. Appl. Catal. B 49 (1), 1–14.

Lachheb, H., Puzenat, E., Houas, A., Ksibi, M., Elaloui, E., Guillard, C., et al., 2002. Photocatalytic degradation of various types of dyes (Alizarin S, Crocein Orange G, Methyl Red, Congo Red, Methylene Blue) in water by UV-irradiated titania. Appl. Catal. B 39 (1), 75–90.

Liu, S.X., Chen, X.Y., 2008. A visible light response TiO_2 photocatalyst realized by cationic S-doping and its application for phenol degradation. J. Hazard. Mater. 152 (1), 48–55.

Liu, Z., Sun, D.D., Guo, P., Leckie, J.O., 2007. An efficient bicomponent TiO_2/SnO_2 nanofiber photocatalyst fabricated by electrospinning with a side-by-side dual spinneret method. Nano Lett. 7 (4), 1081–1085.

Marugán, J., Hufschmidt, D., Sagawe, G., Selzer, V., Bahnemann, D., 2006. Optical density and photonic efficiency of silica-supported TiO_2 photocatalysts. Water Res. 40 (4), 833–839.

Miao, F.X., Deng, Z.H., Lü, X.S., Gu, G.X., Wan, S.M., Fang, X.D., et al., 2010. Fundamental properties of $CdFe_2O_4$ semiconductor thin film. Solid State Commun. 150 (41–42), 2036–2039.

Qiu, J.X., Wang, C.Y., Gu, M.Y., 2004. Photocatalytic properties and optical absorption of zinc ferrite nanometer films. Mater. Sci. Eng. B 112 (1), 1–4.

Ren, W.J., Ai, Z.H., Jia, F.L., Zhang, L.Z., Fan, X.X., Zou, Z.G., 2007. Low temperature preparation and visible light photocatalytic activity of mesoporous carbon-doped crystalline TiO_2. Appl. Catal. B 69 (3–4), 138–144.

Sakthivel, S., Shankar, M.V., Palanichamy, M., Arabindoo, B., Bahnemann, D.W., Murugesan, V., 2004. Enhancement of photocatalytic activity by metal deposition: characterisation and photonic efficiency of Pt, Au and Pd deposited on TiO_2 catalyst. Water Res. 38 (13), 3001–3008.

Sato, J., Saito, N., Nishiyama, H., Inoue, Y., 2001. Photocatalytic activity for water decomposition of RuO_2-loaded $SrIn_2O_4$ with d(10) configuration. Chem. Lett. (9), 868–869.

Selvaraj, A., Sivakumar, S., Ramasamy, A.K., Balasubramanian, V., 2013. Photocatalytic degradation of triazine dyes over N-doped TiO_2 in solar radiation. Res. Chem. Intermed. 39 (6), 2287–2302.

Singh, G., Kapoor, I.P.S., Dubey, R., Srivastava, P., 2010. Preparation, characterization and catalytic behavior of $CdFe_2O_4$ and Cd nanocrystals on AP, HTPB and composite solid propellants, Part: 79. Thermochim. Acta 511 (1–2), 112–118.

Sun, Y.P., Thornton, J.M., Morris, N.A., Rajpura, R., Henkes, S., Raftery, D., 2011. Photoelectrochemical evaluation of undoped

and C-doped $CdIn_2O_4$ thin film electrodes. Int. J. Hydrogen Energy 36 (4), 2785–2793.

Szilágyi, I.M., Fórizs, B., Rosseler, O., Szegedi, A., Németh, P., Király, P., et al., 2012. WO_3 photocatalysts: influence of structure and composition. J. Catal. 294, 119–127.

Tang, J.W., Zou, Z.G., Yin, J., Ye, J., 2003. Photocatalytic degradation of methylene blue on $CaIn_2O_4$ under visible light irradiation. Chem. Phys. Lett. 382 (1–2), 175–179.

Tasbihi, M., Kete, M., Raichur, A.M., Tušar, N.N., Štangar, U.L., 2012. Photocatalytic degradation of gaseous toluene by using immobilized titania/silica on aluminum sheets. Environ. Sci. Pollut. 19 (9), 3735–3742.

Wang, T.X., Xu, S.H., Yang, F.X., 2012. $ZnIn_2S_4$ nanopowder as an efficient visible light-driven photocatalyst in the reduction of aqueous Cr(VI). Mater. Lett. 83, 46–48.

Wu, H.M., Ma, J.Z., Zhang, C.B., He, H., 2014. Effect of TiO_2 calcination temperature on the photocatalytic oxidation of gaseous NH_3. J. Environ. Sci. 26 (3), 673–682.

Xiang, Q.J., Yu, J.G., Jaroniec, M., 2012. Synergetic effect of MoS_2 and graphene as cocatalysts for enhanced photocatalytic H_2 production activity of TiO_2 Nanoparticles. J. Am. Chem. Soc. 134 (15), 6575–6578.

Xu, X.X., Azad, A.K., Irvine, J.T.S., 2013. Photocatalytic H_2 generation from spinels $ZnFe_2O_4$, $ZnFeGaO_4$ and $ZnGa_2O_4$. Catal. Today 199, 22–26.

Zhang, X.T., Udagawa, K., Liu, Z.Y., Nishimoto, S., Xu, C.S., Liu, Y.X., et al., 2009. Photocatalytic and photoelectrochemical studies on N-doped TiO_2 photocatalyst. J. Photochem. Photobiol. A 202 (1), 39–47.

Zhang, Y.H., Zhang, N., Tang, Z.R., Xu, Y.J., 2012. Graphene transforms wide band gap ZnS to a visible light photocatalyst. The new role of graphene as a macromolecular photosensitizer. ACS Nano 6 (11), 9777–9789.

Zou, Z., Ye, J., Arakawa, H., 2000. Preparation, structural and photophysical properties of Bi_2InNbO_7 compound. J. Mater. Sci. Lett. 19 (21), 1909–1911.

Editorial Board of Journal of Environmental Sciences

JOURNAL OF ENVIRONMENTAL SCIENCES

环境科学学报(英文版)

www.jesc.ac.cn

Aims and scope

Journal of Environmental Sciences is an international academic journal supervised by Research Center for Eco-Environmental Sciences, Chinese Academy of Sciences. The journal publishes original, peer-reviewed innovative research and valuable findings in environmental sciences. The types of articles published are research article, critical review, rapid communications, and special issues.

The scope of the journal embraces the treatment processes for natural groundwater, municipal, agricultural and industrial water and wastewaters; physical and chemical methods for limitation of pollutants emission into the atmospheric environment; chemical and biological and phytoremediation of contaminated soil; fate and transport of pollutants in environments; toxicological effects of terrorist chemical release on the natural environment and human health; development of environmental catalysts and materials.

For subscription to electronic edition

Elsevier is responsible for subscription of the journal. Please subscribe to the journal via http://www.elsevier.com/locate/jes.

For subscription to print edition

China: Please contact the customer service, Science Press, 16 Donghuangchenggen North Street, Beijing 100717, China. Tel: +86-10-64017032; E-mail: journal@mail.sciencep.com, or the local post office throughout China (domestic postcode: 2-580).

Outside China: Please order the journal from the Elsevier Customer Service Department at the Regional Sales Office nearest you.

Submission declaration

Submission of the work described has not been published previously (except in the form of an abstract or as part of a published lecture or academic thesis), that it is not under consideration for publication elsewhere. The publication should be approved by all authors and tacitly or explicitly by the responsible authorities where the work was carried out. If the manuscript accepted, it will not be published elsewhere in the same form, in English or in any other language, including electronically without the written consent of the copyright-holder.

Editorial

Authors should submit manuscript online at http://www.jesc.ac.cn. In case of queries, please contact editorial office, Tel: +86-10-62920553, E-mail: jesc@rcees.ac.cn. Instruction to authors is available at http://www.jesc.ac.cn.

Journal of Environmental Sciences (Established in 1989)
Volume 29 2015

Supervised by	Chinese Academy of Sciences	**Published by**	Science Press, Beijing, China
Sponsored by	Research Center for Eco-Environmental		Elsevier Limited, The Netherlands
	Sciences, Chinese Academy of Sciences	**Distributed by**	
Edited by	Editorial Office of Journal of	Domestic	Science Press, 16 Donghuangchenggen
	Environmental Sciences		North Street, Beijing 100717, China
	P. O. Box 2871, Beijing 100085, China		Local Post Offices through China
	Tel: 86-10-62920553; http://www.jesc.ac.cn	Foreign	Elsevier Limited
	E-mail: jesc@rcees.ac.cn		http://www.elsevier.com/locate/jes
Editor-in-chief	X. Chris Le	**Printed by**	Beijing Beilin Printing House, 100083, China

CN 11-2629/X **Domestic postcode: 2-580** **Domestic price per issue RMB ¥ 110.00**

ISSN 1001-0742